Traffic Induced Changes in Small-Strain Stiffness of Geogrid Stabilised Aggregate

Chelsey Yesnik, Igor Morozov, Haithem Soliman, I.R. Fleming, Ethan Landry & Adam Hammerlindl
Department of Civil, Geological, and Environmental Engineering - University of Saskatchewan, Saskatoon, Saskatchewan, Canada

ABSTRACT

Geogrid stabilisation preserves the aggregate stiffness and reduces permanent deformations in roadways. The stiffness enhancement varies with depth relative to the aggregate/geogrid interface. Multichannel analysis of surface waves (MASW) can be used to measure the aggregate stiffness at high resolutions across the aggregate layer. Preliminary testing was completed at the Saskatchewan Soft Soil Subgrade Stabilisation Study Site to optimize the test parameters for MASW in geogrid stabilised and non-stabilised aggregates. A full-scale wheel trafficker system will apply accelerated traffic loading to four geogrid-stabilised test sections, and one non-stabilised test section. MASW will be completed with multiple accelerometers arrays to measure the aggregate stiffness with time and distance relative to the applied load.

RÉSUMÉ

La stabilisation de la géogrille préserve efficacement la rigidité des agrégats et réduit les déformations permanentes dans les galeries. Des études antérieures ont confirmé que cette amélioration de la rigidité varie en fonction de la profondeur par rapport à l'interface agrégat/géogrille. L'analyse d'ondes de surface multicanal (MASW) peut être utilisée pour mesurer la rigidité des agrégats à des résolutions élevées à travers la couche agrégée. Des essais préliminaires ont été effectués sur le site de l'étude de stabilisation des sols mous de la Saskatchewan afin d'optimiser les paramètres d'essai de l'ASM dans les agrégats stabilisés et non stabilisés de la géogrille. Un système de circulation des roues à grande échelle récemment mis en service appliquera une charge de trafic accélérée à quatre sections d'essai stabilisées à la géogrille et à une section de commande non stabilisée. MASW sera complété par plusieurs réseaux d'accéléromètres pour mesurer l'évolution de la rigidité globale au fil du temps et de la distance par rapport à la charge appliquée.

1 INTRODUCTION

Geogrid stabilisation helps preserve the aggregate stiffness in roadways subject to short- and long-term traffic loading (Zornberg & Roodi 2021); though, it has been found that this stiffness enhancement decreases with increasing height above the geogrid (Byun et al. 2019, Kang, et al. 2022). It is the objective of this research is to define a near-continuous stiffness profile with depth through the aggregate at various cyclic loading intervals. Traffic loading will be applied to test sections using a full-scale wheel trafficker system. The performance of four widely available geogrids, with similar aperture geometry and varying rib thickness, will be evaluated. A non-stabilised control section will also be assessed. The stiffness profile will be measured at locations both directly beneath and adjacent to the applied traffic load using a seismic technique. The goal is to identify any recognizable trends in the measured stiffness profiles with respect to the number of load cycles applied, relative distance to the applied load, and differences in geogrid properties. This is a multi-year project, which will also include a co-related study comparing the severity of rutting amongst stabilised and non-stabilised test sections.

2 BACKGROUND

Rutting is the result of permanent deformations in the road structure and subgrade, which are caused by the following two failure mechanisms: lateral spreading of the aggregates, and bearing capacity failure in the subgrade (Giroud & Han 2004, Zornberg et al. 2017, Lees 2017). Lateral spreading is the displacement of granular particles in the aggregate layers when subject to traffic load due to a lack of particle interlock. The resulting decrease in particle confinement causes the aggregate stiffness to degrade, which gives rise to less effective load transfer from the aggregate to the subgrade (Zornberg 2017). Subsequently, the loss in particle interlock within the aggregate results in less surcharge transfer development to resist subgrade shearing and heave (Lees 2017), as shown in Figure 1A.

The aggregate layers can be stabilised to help preserve the initial stiffness of the aggregate by minimizing permanent deformations and lateral spreading of the aggregates. Stabilisation also reduces the cost and frequency of road maintenance and rehabilitation efforts. Stabilisation can be achieved by using higher-quality aggregates with increased frictional resistance; however, good quality aggregates cannot always be sourced in every jurisdiction. Aggregates are also a rapidly depleting, non-renewable resource, which exaggerates the need for alternative methods to achieve stabilisation.

Geogrids can be used to stabilise aggregates when installed either within the aggregate layer, and/or at the aggregate/subgrade interface. A high degree of interaction between the aggregate particles and geogrid apertures is required for stabilisation to be successful. This ensures the effective transfer of shear stresses from the aggregate to tensile stresses in the geogrid. Stress transfer is mobilized

at small strains/displacements in the geogrid, which initiates during construction and initial traffic loading (Zornberg 2017). Effective particle interlock also helps counterbalance any potential bearing capacity failure in the subgrade (Lees 2017), as shown in Figure 1B. In addition to preserving the aggregate stiffness, stabilisation can also reduce the thickness of base course required for design; thus, providing a sustainable solution to preserving non-renewable aggregate resources (Zornberg & Roodi 2021).
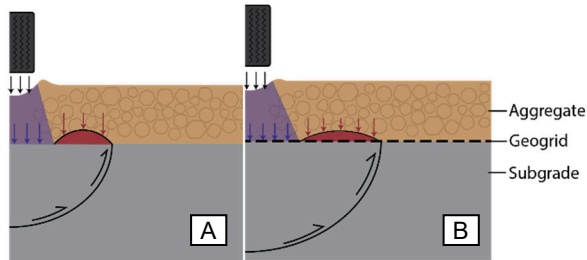

Figure 1. Subgrade shearing and heave: (A) without geogrid, and (B) with geogrid

Geogrid-stabilised roadway design and performance is traditionally evaluated using one or more of the following metrics: traffic benefit ratio (TBR); and/or base course reduction (BCR) (Berg et al. 2000). Geogrid manufacturers often provide these values within their product specification sheets; however, these performance metrics are a function of the specific road design and geosynthetic materials selected for testing. Therefore, the TBR and BCR are often not comparable amongst different geogrid products, as manufacturer test conditions are usually non-consistent with one another.

Consequently, many researchers and transportation agencies have completed independent studies to predict and quantify the stiffness enhancement achieved through geogrid stabilisation. For a specific roadway design, these studies are usually completed through index testing, analytical models, and/or performance testing.

Index tests often assess the mechanical and physical properties of the geogrid in isolation. However, the geogrid should be evaluated while in contact with the project aggregate to simulate the composite behavior developed through enhanced particle interlock and stress transfer mechanisms (Archer & Wayne 2012, Zornberg et al. 2017). Many different analytical models and boundary conditions have also been developed to represent the soil-geogrid interaction. Though, analytical models are usually complex, which inherently requires the use of numerical models to find a solution (Lees 2017).

Performance tests offer an empirical-based approach to help designers select an appropriate geogrid type, installation depth, and aggregate properties for their project. These tests are completed through larger-scale laboratory tests, constructed test sections, and/or field testing. There are many performance tests in literature that have yielded meaningful observations and general trends (Cuelho & Perkins 2009, Cuelho et al. 2014, Cuelho & Perkins 2017, Zornberg et al. 2017, Byun et al. 2019, Zornberg & Roodi, 2021, Kang, et al. 2022). Though, the results from performance tests are limited to the specific road design (i.e., layer thicknesses, aggregate and subgrade properties, and geogrid properties), traffic loading, and environmental loading (i.e., temperature and moisture content). Additionally, the stiffness enhancement is usually only measured at few discrete depths within the aggregate layer (Byun et al. 2019, Kang et al. 2022).

Therefore, it is important that the current knowledge base is continually expanded by testing geosynthetics with a variety of aggregates and subgrade soils, subject to various loading conditions (Cuelho & Perkins 2017). A better understanding of the stiffness enhancement with depth can also help agencies more accurately predict the long-term performance and cost benefits of geogrid stabilisation.

.

3 SEISMIC TECHNIQUES

3.1 Shear Wave Velocity and Small Strain Shear Modulus

Following seismic activity, body waves and surface waves propagate through the earth and along its surface. Body waves are comprised of compression waves and shear waves. Compression waves create a particle motion that is parallel to the direction of wave travel, while shear waves create a particle motion that is perpendicular to the direction of wave travel. Surface waves are comprised of both Rayleigh and Love waves. Rayleigh waves are produced by the interaction between compression waves and the vertical component of shear waves (Aki & Richards, 1980). Love waves are created by the interaction between the horizontal component of shear waves, and a low velocity surface layer (Everett 2013).

Of the several types of seismic waves, only shear waves can be used to characterize the stiffness of soil. Compression waves can travel through both soil and water; however, shear waves can only be transmitted through the soil skeleton. Using elastic theory, Eq. 1 is developed for small strain shear modulus, G_{max}, with respect to the soil density, ρ, and the velocity of a shear wave travelling through the soil, V_s (Kang et al. 2022).

$$G_{max} = \rho V_s^2 \qquad [1]$$

3.2 Surface Wave Analysis

Seismic techniques can be used to measure the shear wave velocity and corresponding aggregate stiffness through the aggregate. Surface wave analysis causes minimal soil disturbance and maximizes the ease and versatility of sensor installation. Surface wave analysis methods are dependent on the dispersive nature of the surface waves travelling in a vertically heterogenous soil medium. Rayleigh waves are used for surface wave analysis since they are easy to generate and detect across the soil surface using only low-frequency seismic sensors (Everett 2013). In a homogenous medium, the Rayleigh wave velocity is non-dispersive, and independent of the wave frequency. Though, Rayleigh waves disperse in a heterogenous (layered) soil profile with varying stiffness, which results in numerous wave components.

Each wave component has its own wavelength, frequency, penetration depth and velocity (Aki & Richards 1980). The velocity at which each individual wave component propagates is referred to as the phase velocity, c. The relationship between wave frequency (f), Rayleigh wave phase velocity (c(f)), and wavelength (λ(f)) through a heterogeneous medium can be described using Eq. 2 (Park 2011).

$$\lambda(f) = \frac{c(f)}{f} \qquad [2]$$

The Rayleigh wave phase velocity will depend on the material properties across the entire depth through which the wave travels. Different frequency waves can access and measure soil properties at various depths (Park 2018), as seen in Figure 2 below. Shorter, high frequency waves will propagate through the upper layers of the soil, while longer, low frequency waves will propagate to greater depths within the soil. By measuring both high and low frequency waves, the V_s at various depths and corresponding stiffness profile (G_{max}) can be determined.
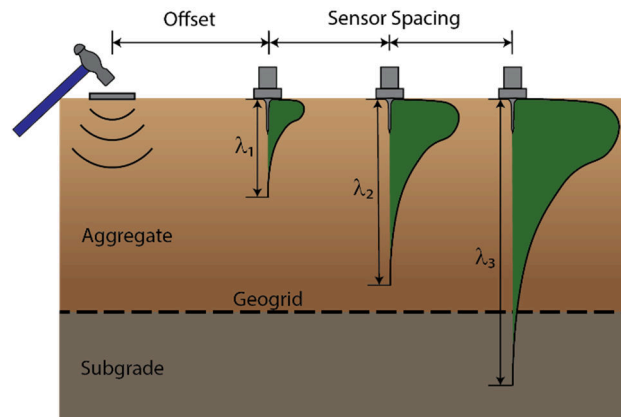

Figure 2. Surface wave analysis through aggregate soil

Surface wave analysis is comprised of three main components (Ryden et al. 2004):

1) Completing field measurements to obtain the raw surface wave records,
2) Processing the surface wave records to determine the experimental dispersion curves, and
3) Estimating the soil stiffness with depth through inversion of the experimental dispersion curves.

The experimental dispersion curves represent the relationship between c(f) and f. Rayleigh waves travelling at different frequencies can share the same c(f). The lowest c(f) measured for a certain f is called the fundamental mode phase velocity. Any c(f) faster than the fundamental mode velocity is considered a higher mode (Xia et al. 2003). Subsequent inversion analysis is then completed with all of the fundamental mode phase velocities to estimate V_s with depth for a particular soil profile (Park et al. 2018).

Multichannel analysis of surface waves (MASW) has been selected for this research to measure the stiffness profile through the aggregate. MASW was developed as an improvement to the more subjective and labour-intensive spectral analysis of surface waves (SASW). MASW typically uses up to 24 vibration sensors in an array (or more), where SASW typically uses no more than 12 vibration sensors. Therefore, the upfront cost of sensors and multichannel data acquisition equipment is greater for MASW than SASW (Davis, 2016).

However, MASW offers a faster and less subjective separation of different modes, mitigates near-field effects, and enables the detection of different fundamental modes (Park 2011). Therefore, MASW is ideal for analyzing pavement structures, as soil stiffness can be measured at high resolutions over shallow depths (Park et al. 2018).

3.3   Vibration Sensors

Geophones are low frequency vibration sensors, which can measure frequencies of up to 1-2 kHz (Park et al. 2018). Accelerometers are high frequency vibration sensors which are capable of measuring frequencies of up to 10-20 kHz, or greater (Davis 2016). The choice to use geophones or accelerometers for MASW depends on the desired depth of analysis and measurement resolution.

Park (2018) states that geophones are practical for measuring low frequency waves found at greater depths (e.g., between 1 and 30 metres). They are also more robust and less costly than accelerometers. Though, Park (2018) also states that geophones tend to underestimate the high frequency waves travelling at shallow depths (e.g., less than a metre). As a result, the V_s at shallow depths is also underestimated. Accelerometers are capable of measuring high frequencies, and can offer finer resolution measurements of V_s with depth than geophones (Park et al. 2018). Therefore, accelerometers will be used for this research to complete MASW.

3.4 Equipment Requirements and Layout

The test parameters for MASW must be optimized for each specific test site. These parameters include the source type/size, source offset, sensor type, number of sensors (i.e., array length), and sensor spacing (Ferreira et al. 2014). The size/type of source will affect the Rayleigh wave frequency and the corresponding modes appearing on the experimental dispersion curves (Foti et al. 2018).

The source offset influences the near- and far-field effects on the measured surface wave record, which also impacts the experimental dispersion curve. The measurable frequency range is governed by the type of sensors, number of sensors, and sensor spacing. Additionally, the sensor spacing, and number of sensors will control the measurement resolution and depth, respectively (Park 2011). Longer sensor spacing increases the measurement accuracy for low frequency waves, while shorter sensor spacing increases the measurement accuracy for high frequency waves (Xia et al. 2003). In general, the length of the sensor array should be two to three times greater than the maximum desired wavelength (Foti et al. 2018).

Accelerometer sensitivities are typically selected between 100-500 mV/g, with a maximum frequency response of 20-25 kHz, or higher (Park 2011). There is usually minimal explanation provided in literature as to how the accelerometer sensitivity is selected. However, the measurable frequency response is usually selected with respect to soil material properties, and desired measurement depth and resolution. The mounting configuration is dependent on the soil surface over which the accelerometers must be coupled with for testing. Adhesive and magnetic mounting techniques are typically used for paved roads, while pin (nail) mounting techniques are typically used for soils (Ryden et al. 2004). The cables can be connected to either the top or side of the accelerometer, which depends on where the accelerometers are being mounted and cable organization.

4 EXPERIMENTAL PROGRAM

4.1 Full-Scale Wheel Trafficker System

A full-scale wheel trafficker system has been recently commissioned at the University of Saskatchewan as shown in Figure 3. This system is comprised of a structural steel exoskeleton which houses an epoxy-laminated, five-layer marine plywood box. The box dimensions are 6.10 m long by 2.82 m wide, which can accommodate 4 – half-lane test sections at once.

The steel exoskeleton provides support to the traffic loading system, and minimizes any outward movement of the box walls during soil placement and trafficking. The box is also insulated to reduce temperature fluctuations in the soil, and noise during MASW testing. A human-machine interface allows for real-time control and monitoring of load, wheel position and cycling speed. Nine system variables can be pre-set, or manually adjusted to tune the system performance. The traffic loading system is comprised of two 255/70R22.5 semi truck tires which apply a pneumatic load to the surface of the aggregate.

The pneumatic loading system contains 2 carriage houses, each equipped with pneumatic cylinders which are pressurized to 90 psi. The applied pressure of 90 psi is equal to one-half of an equivalent single axle load (ESAL). Three air compressors, equipped with HMI controlled pneumatic directional valves, provide air flow for the application of cyclic vertical load. A 7.5 kW servo motor and gear box then deliver power to a dual-chain drive to propel the wheel set across the aggregate surface. Stopping power is applied to the semi tire wheel set using a 500 W braking resistor.

During trafficking, the semi tire set will begin in a raised position at the beginning of the test section. The wheels will then start to move forward along the length of the test section, while gradually lowering. Once in contact with the aggregate surface, the wheels will travel over the surface while applying a half-ESAL traffic load. After the wheels have travelled almost the entire length of the test section, they will gradually raise and stop before contacting the box wall. In the fully raised position, the wheel position will be reset to the beginning of the test section. A total of 1200 cycles will be completed at a fifteen-second nominal cycle

time, which includes lowering, travelling, raising, stopping and resetting the semi tire set. The trafficking pattern is shown in Figure 3, where the blue and red arrows represent forward and backward motion, respectively.
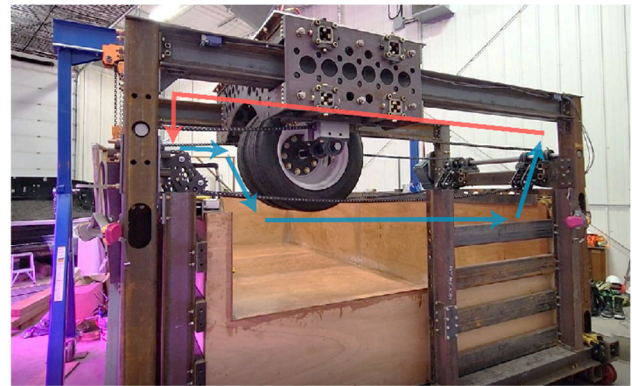

Figure 3. Full-scale wheel trafficker system, with traffic loading pattern

4.2 Materials

4.2.1 General Description of Test Section

Each test section will be approximately 2.82 m long (in the direction of trafficking) by 1.52 m wide (perpendicular to trafficking). For this study, five different unsurfaced road sections will be evaluated: four geogrid-stabilised test sections, each containing a different geogrid product; and 1 control section, with no geogrid stabilisation. The geogrids will have similar aperture size and shape; however, the rib thickness is different for each product. Multiple installations will be completed in the full-scale wheel trafficker to evaluate all test sections. Furthermore, each test section will be installed and evaluated in more than one location to minimize any discrepancies in test section performance due to wall boundary effects.

Each test section will be built as an unsurfaced road using the following materials, listed in order of placement: Two - 9 oz. non-woven geotextiles, a uniform sand capillary break (1-2 in.), an artificial subgrade (600 mm), and a special blend aggregate (300 mm). The sand capillary break will provide moisture control across the subgrade soil using an adjustable head reservoir.

Eighteen well-sealed PVC ports, installed along the box walls, will facilitate the measurement of spatial and temporal changes in subgrade moisture conditions using tensiometers. Pressure cells are embedded within the sand to measure the stress directly beneath the applied traffic load, and at the internal edge of each test section. An illustrative cross-section, showing a typical geogrid-stabilised test section within the full-scale wheel trafficker system, can be seen in Figure 4 below.

4.2.2. Subgrade

An artificial clay subgrade material was selected for this research, as to minimize any discrepancy in test section performance. The selected material is a Plainsman Buffstone kaolinite clay, purchased from Plainsman Clays in Medicine Hat, Alberta. Table 1 represents some of the characteristics of the artificial clay subgrade material.

Table 1. Properties of artificial subgrade material

Characteristics	Values
Liquid Limit (%)	34.5
Plastic Limit (%)	16.9-17.7
Water Content (%)	20.8-24.7
Undrained Shear Strength, S_u (kPa)	22-43

Atterberg testing (ASTM D4318) was completed to obtain the liquid limit and plastic limit of the artificial subgrade material. The water content of the clay slug was also measured immediately after opening the sealed samples. Undrained shear strength (S_u) was measured using laboratory shear vanes. The artificial clay subgrade will be hand placed directly over the sand capillary break. The subgrade will then be manually compacted until uniform strength is achieved across all test sections. The compaction effort will be closely monitored as to not exceed the bearing capacity of the clay.

4.2.3. Aggregate

A Type 32 special blend (T32-SB) aggregate was selected for this research. This material is comprised of locally sourced aggregates, crushed to 90% one-face fracture and 60% two-face fracture. The T32-SB aggregate is similar to the Type 31 (T31) and Type 33 (T33) granular base course used by the Saskatchewan Ministry of Highways (Government of Saskatchewan 1996). Though, T31 and T33 granular base course is finer and less fractured (only 50% minimum fracture) than the T32-SB. The grainsize distribution (GSD) for the T32-SB, T31, and T33 can be seen in Figure 5. The aggregate will be placed and compacted in approximately 2-3 lifts using a plate tamper. The base aggregate density will be verified through nuclear densometer testing at multiple locations across each test section.

4.3   Accelerometers and Data Acquisition

In 2021, preliminary surface wave analysis was completed at the Saskatchewan Soft Soil Subgrade Stabilisation Study Site (S7) near Clavet, SK. The goal of this testing was to evaluate and select the best-suited accelerometer properties prior to testing in the full-scale wheel trafficker system.

A variety of source sizes, source offsets, and sensor spacings were tried. The testing was completed over two field test sections: a geogrid-stabilised test section and non-stabilised test section. Each test section was built with 300 mm of special blend aggregate, overlying a soft, silty clay subgrade. The clay subgrade has an average small-strain shear modulus of approximately 35 MPa (at 1.5-2.5 m depth). The special blend aggregate has an optimum density of 2220 kg/m^3 at 7.1% water content. The GSD for the special blend aggregate (S7 Special Blend) can be seen in Figure 5. A triangular aperture geogrid, with a 40 mm pitch, was placed at the aggregate-subgrade interface in the stabilised test section.
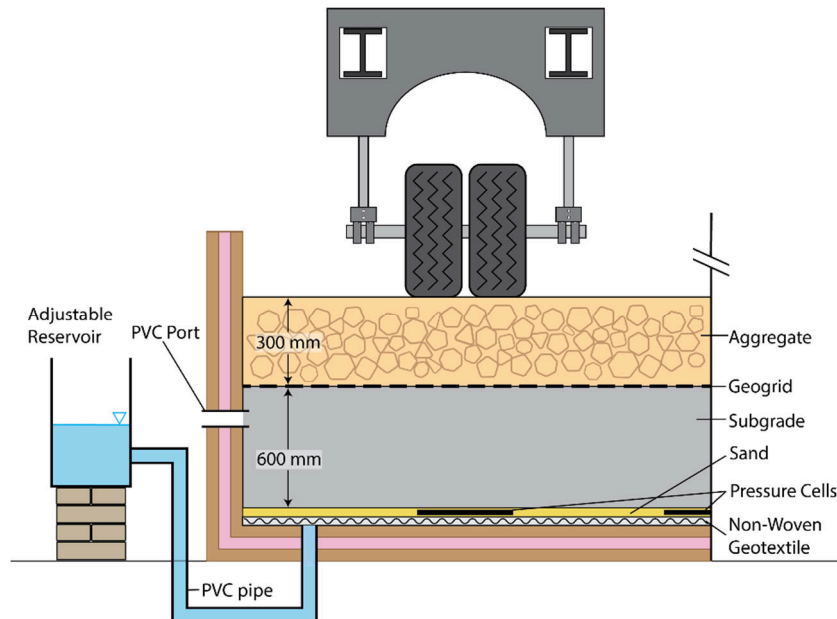

Figure 4. Stabilised test section in full-scale wheel trafficker system
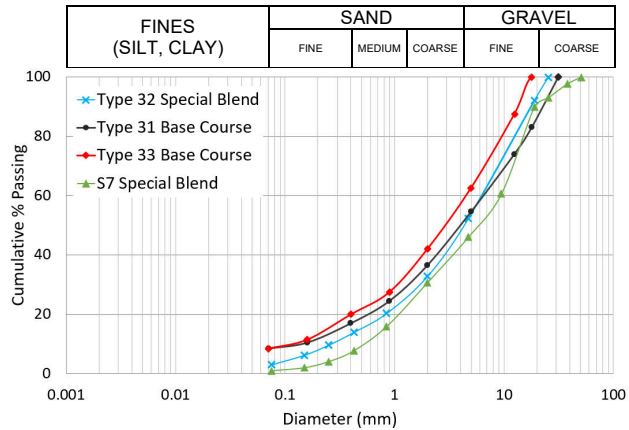
Figure 5. GSD for aggregate materials

A CTC AC102-1A multipurpose accelerometer, CTC AC133-1D low frequency accelerometer, and Wilcoxon WR-736T Miniature Accelerometer were selected for testing. The sensitivity and frequency (freq.) response of each accelerometer can be seen in Table 2. Each accelerometer is stud mounted to a 1" mounting disk with an attached 2" spike that will be pushed into the aggregate. The accelerometers are tested in various positions within the array at 5, 10, and 15 cm spacing.

Table 2. Accelerometer properties

Specifications	AC102-1A	AC133-1D	WR-736T
Sensitivity (mV/g)	100	500	100
Freq. Response (Hz)[1]	0.5-15,000	0.1-10,000	2-25,000

[1]measured over +/- 3 dB

Five ball pein hammers, ranging in size from 227 g – 907 g, were each struck against a metal plate to create a unique, high-frequency wave source. Attached to each hammer is a high g-force accelerometer to measure the approximate time of strike. The source offsets are varied between 12.5 to 150 cm. All accelerometer measurements are read using a National Instruments Data Acquisition system (DAQ). The DAQ connects to a laptop which records and processes the raw signals in MATLAB. The general test setup is shown in Figure 6 below.

Figure 6. Preliminary surface wave analysis at S7

5   RESULTS AND DISCUSSION

5.1   Raw Signal and Spectra

Over 200 trials were completed at S7 to evaluate the selected accelerometers. Trials were completed in the same location for each test section to minimize any discrepancies in the results. A maximum sampling frequency of 51,200 Hz was used to measure and record the raw accelerometer signal. Subsequently, the frequency spectra (amplitude vs. frequency) was plotted for each accelerometer in the array. From the frequency spectra, the measured frequency through the aggregate material was approximated. A longer accelerometer array is required to complete dispersion and inversion analysis. Though, the initial cost of accelerometers is quite high. A full, 24-geophone array was placed alongside the accelerometers to obtain an initial estimate of Vs. An array of 24 Hz geophones and 100 Hz geophones was tried, as to maximize the geophone frequency response.

The frequency spectra for two separate accelerometer trials are shown in Figures 7 and 8 below. Figure 7 shows the frequency spectra measured in the non-stabilised aggregate, and Figure 8 shows the frequency spectra measured in the geogrid-stabilised aggregate. Both trials were completed with a 454 g hammer, struck at a 12.5 cm offset from the accelerometer array.
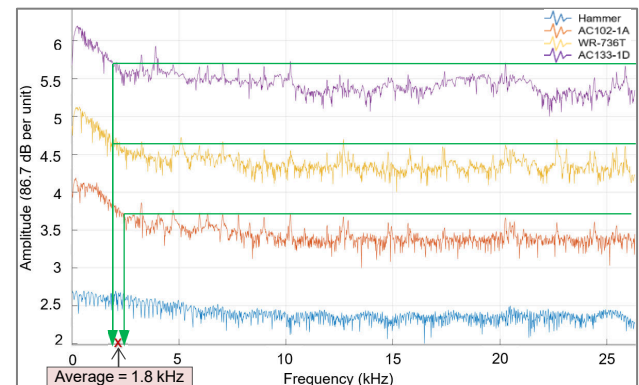

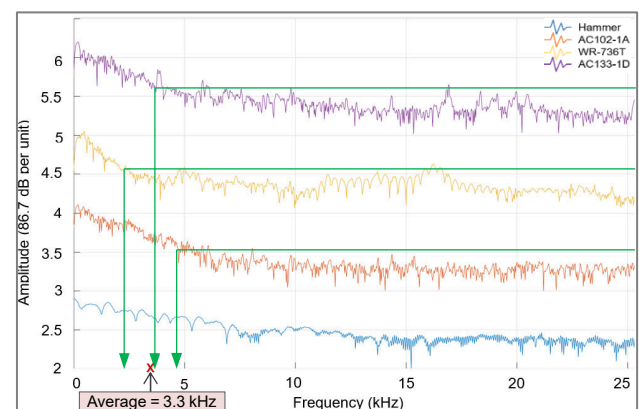Figure 7. Frequency spectra for non-stabilised aggregate

Figure 8. Frequency spectra for stabilised aggregate

The wave signal and frequency generated by the hammer strike is represented by the downward sloping portion of the frequency spectra. On-site noise is then represented as the flattened portion of the frequency spectra. The frequency in the non-stabilised aggregate is measured up to 1.8 kHz (on average). The frequency in the geogrid-stabilised aggregate is measured up to 3.3 kHz (on average). In a similar study, Davis (2016) completes MASW for a variety of soil types, sensor spacings, number of sensors, source sizes, and source offsets. Davis (2016) measures frequencies up to 1.7 kHz in a fine-grained soil comprised mostly of silt. Davis (2016) also measures frequencies up to (and exceeding) 4kHz in asphalt concrete. The measured frequencies from Davis (2016) are comparable to the frequencies measured at S7 in the non-stabilised and geogrid-stabilised aggregates. It is hypothesized that the difference in measured frequencies between the two test sections may be related to inconsistencies in the subgrade material and/or the stiffness enhancement created by the geogrid.

Through preliminary dispersion analysis, there is a notable variance in Vs measured with depth in the stabilised section. For the upper 10 cm, Vs is approximately equal to 100 m/s. At 1 m below the surface (in the clay subgrade), Vs is approximately 300-400 m/s. Detailed inversion analysis with high-resolution accelerometers is required to determine how Vs varies with depth at finer increments.

All three accelerometers had comparable performance. Though, some accelerometers were more sensitive to on-site noise than others. On-site noise included strong wind gusts, and nearby operating machinery. The accelerometer sensitivity should be at least 100 mV/g, which is similar to previous studies (Park 2011). It is also recommended that the selected accelerometer has a maximum frequency response greater than 4 kHz. Any abnormalities observed in the raw signal, such as signal clipping, are likely related to the source size and offset distance. The raw accelerometer signals were most clear for the 227- 454 g hammers, at source offsets ≤ 75 cm. The top exit configuration created difficulties in cable organization, and caused the accelerometers to lean out of plumb. Therefore, it is recommended that side exit accelerometers are used going forward.

5.2 Proposed Instrumentation Plan and Procedure

Fifteen CTC AC104-1A multipurpose accelerometers have been selected for the full-scale wheel trafficker experiment. The accelerometers have 100 mV/g sensitivity, with a 0.5 – 10,000 Hz frequency response. Each accelerometer will be stud mounted to a 1" mounting disk with an attached 2" spike. A 227 g ball-pin hammer, equipped with a high g-force accelerometer, will be used to generate surface waves throughout the base course layer. A source offset of 30 cm will be used.

MASW testing will be completed incrementally after the following number of load cycles: 0, 40, 120, 400, 750, and 1200 load cycles. Four accelerometer arrays will be used for the analysis, as shown in Figure 9. Each accelerometer array will be 0.7 m in length, with 5 cm spacing between the accelerometers. One array will be installed in the wheel path, and three arrays will be installed approximately 45, and 65 cm offset from the centre of the semi tire set. By installing the arrays in various locations relative to the traffic load, spatial variations in the stiffness profile can be determined. There are enough mounting disks installed for all four arrays. The mounting disks will be installed once (prior to loading). The accelerometers can be moved to alternate array locations while maintaining the same sensor positioning as in earlier tests.
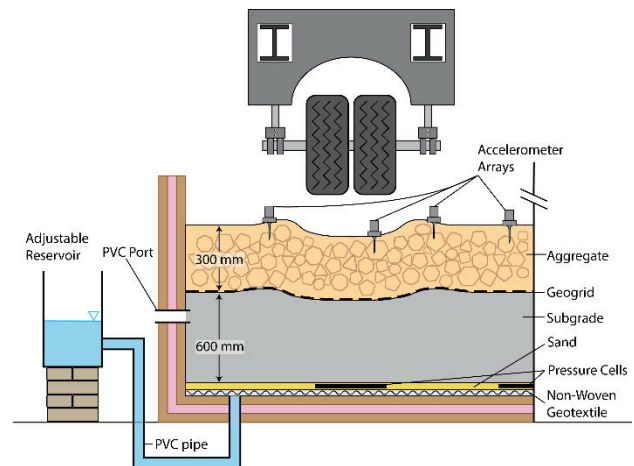

Figure 9. Accelerometer array positions

6 CONCLUSION

Preliminary surface wave analysis was completed over a geogrid-stabilised and non-stabilised aggregate overlying a soft, silty clay subgrade. Three different accelerometers were evaluated, as well as a variety of source sizes, source offsets, and sensor spacings. The frequency measured in the stabilised and non-stabilised aggregate was 1.8 kHz and 3.3 kHz, respectively. The measured frequencies were comparable to those measured in a similar MASW study (Davis 2016). Differences in measured frequency could be attributed to variable material properties, and/or the possible stiffening enhancement fostered by geogrid stabilisation. Preliminary measurements of Vs were also obtained, which confirms that the initial aggregate stiffness with depth can be measured prior to traffic loading.

A full-scale wheel trafficker system will be used to determine the spatial and temporal changes in aggregate stiffness with depth once subject to traffic load. Four geogrid-stabilised test sections, and one control section will be evaluated using MASW. Four accelerometer arrays will be positioned across the aggregate surface at locations beneath and adjacent to the applied traffic load. It is anticipated that the aggregate stiffness will increase with proximity to the soil-geogrid interface once exposed to short-term traffic loading. This geogrid stiffening effect will be the greatest near the applied load.

It is anticipated that the aggregate stiffness between geogrid-stabilised and non-stabilised test sections may vary initially (prior to loading). If the variability in stiffness is not apparent initially, differences in aggregate stiffness will likely become more pronounced as loading progresses.

The stiffness profile will be characterized by changes in Vs through the aggregate, as compared to the initial Vs measured prior to trafficking. The non-stabilised aggregate may experience more rapid deterioration of aggregate stiffness than the geogrid-stabilised sections once subject to cyclic traffic loading.

7 ACKNOWLEDGEMENTS

8 REFERENCES

Aki K. and Richards, P.G. 1980. Quantitative Seismology: Theory and Methods, *W.H. Freeman & Co.,* New York, NY, USA.

ASTM. 2017. D4318-17e1: Standard Test Methods for Liquid Limit, Plastic Limit, and Plasticity Index of Soils, *ASTM International*, West Conshohocken, PA, USA.

Archer, S. and Wayne, M.H. 2012. Relevancy of Material Properties in Predicting the Performance of Geogrid-Stabilized Roadways, *GeoCongress 2012,* ASCE, Oakland, CA, USA.

Berg, R.R., Christopher, B.R., and Perkins, S. 2000. Geosynthetics Reinforcement of the Aggregate Base/Subbase Courses of Pavement Structures, *Geosynthetics Materials Association White Paper II,* Roseville, MN, USA.

Byun, Y.H., Tutumluer, E., Feng, B., Kim, J.H. and Wayne, M.H. 2019. Horizontal stiffness evaluation of geogrid-stabilized aggregate using shear wave transducers. Geotextiles and Geomembranes, 47(2): 177-186.

Cuelho E. and Perkins S. 2009. Field investigation of geosynthetics used for subgrade stabilization, *Final Report to the Montana Department of Transportation*, FHWA/MT-09-003/8193: 140.

Cuelho E., Perkins S. and Morris Z. 2014. Relative operational performance of geosynthetics used as subgrade stabilization. Final Report to the Montana Department of Transportation, FHWA/MT-14-002/7712-251: 328.

Cuelho E. and Perkins, S. 2017. Geosynthetic subgrade stabilization – Field testing and design method calibration, *Transportation Geotechnics,* 10: 22-34.

Davis, B.J. 2016. Development of the MASW Method for Pavement Evaluation, *ProQuest,* Ann Arbor, MI, USA.

Everett, M.E. 2013. Near-Surface Applied Geophysics, *Cambridge: Cambridge University Press,* New York, NY, USA.

Foti, S., Hollender, F., Garofalo, F., Albarello, D., Asten, M., Bard, P., Comina, C., Cornou, C., Cox, B., Guilio, G.D., Forbriger, T., Hayashi, K., Lunedei, E., Martin, A., Mercerat, D., Ohrnberger, M., Poggi, V., Renalier, F., Sicilia, D., and Socco, V. 2018. Guidelines for the good practice of surface wave analysis: a product of the InterPACIFIC project, *Bulletin of Earthquake Engineering,* 16(6): 2367-2420.

Ferreira, C., Martins, J.P., and Correia, A.G., 2014. Determination of the Small-Strain Stiffness of Hard Soils by Means of Bender Elements and Accelerometers, *Geotechnical and Geological Engineering,* 32: 1369-1375.

Giroud, J.P. and Han, J. 2004. Design Method for Geogrid-Reinforced Unpaved Roads. I. Development of Design Method, *Journal of Geotechnical and Geoenvironmental Engineering,* ASCE, 130(8): 775-786.

Government of Saskatchewan Ministry of Highways. 1996. 3505 – Specification for Granular Base Course, *Publications Saskatchewan,* Regina, SK, CAN.

Kang, M., Qamhia, I.I.A., Tutumluer, E., Flynn, M., Garg, N. and Villafane, W. 2022. Near geogrid stiffness quantification in airport pavement base layers using bender element field sensor, *Proceedings of the 4th International Conference on Transportation Geotechnics,* Springer, Chicago, IL, USA, 165: 703-715.

Lees, A. 2017. Bearing capacity of a stabilised granular layer on clay subgrade, *Proceedings of the 10th International Conference on the Bearing Capacity of Roads, Railways and Airfields:* 1135-1142.

Park, C.B. 2011. Imaging Dispersion of MASW Data – Full vs. Selective Offset Scheme, *Journal of Environmental & Engineering Geophysics,* 16(1): 13-23.

Park, C., Richter, J., Rodrigues, R. and Cirone, A. 2018. MASW applications for road construction and maintenance, *Leading Edge,* Tulsa, OK, USA.

Ryden, N. and Lowe, M.J. 2004. Guided wave propagation in three-layer pavement structures, *The Journal of the Acoustical Society of America,* 116(5): 2902-2913.

Xia, J., Miller, R.D., Park, C.B., and Tian, G. 2003. Inversion of High Frequency Surface Waves with Fundamental and Higher Modes, *Journal of Applied Geophysics,* 52(1): 45-57.

Zornberg, J.G., Roodi, G.H. and Gupta, R. 2017. Stiffness of Soil-Geosynthetic Composite under Small Displacements: I. Model Development, *Journal of Geotechnical and Geoenvironmental Engineering,* ASCE, 143(10): 4017075.

Zornberg, J.G. 2017. Functions and Applications of Geosynthetics In Roadways, *Procedia Engineering,* 189: 298-306.

Zornberg, J.G. and Roodi G. H. 2021. Use of geosynthetics to mitigate problems associated with expansive clay subgrades, *Geosynthetics International,* 28(3): 279-302.